remote sensing

MDPI

Article

Sea Surface Height Estimation from Improved Modified, and Decontaminated Sub-Waveform Retracking Methods over Coastal Areas

Parisa Agar [1], Shirzad Roohi [2], Behzad Voosoghi [1,*], Arash Amini [1] and Davod Poreh [3,4]

[1] Faculty of Geodesy and Geomatics Engineering, K. N. Toosi University of Technology, Tehran 15433-19967, Iran
[2] Satellite System Ground Segments Division, Technical and Scientific Support Department, European Organisation for the Exploitation of Meteorological Satellites (EUMETSAT), Innovation Solution-GMV, 64295 Darmstadt, Germany
[3] Department of Electrical Engineering and Information Technology, University of Napoli Federico II, 80138 Naples, Italy
[4] Electrical Engineering Department, Sharif University of Technology, Tehran 14588-89694, Iran
* Correspondence: vosoghi@kntu.ac.ir

Abstract: Coastal zones are challenging areas for sensing by satellite altimeters because reflected signals from non-water surfaces and from calm sea surfaces in small bays and ports inside the radar footprint lead to erroneous powers in return waveforms. Accordingly, these contaminated waveforms do not follow the so-called Brown model in conventional retracking algorithms and fail to derive qualified ranges. Consequently, the estimated water level is erroneous as well. Therefore, selecting an optimized retracker for post-processing waveforms is significantly important to achieve a qualified water level estimation. To find the optimized retracker, we employed a methodology to minimize the effect of erroneous powers on retracked range corrections. To this end, two new approaches were presented, one based on a waveform decontamination method and the other based on a waveform modification method. We considered the first meaningful sub-waveforms in the decontaminated waveforms and in the modified waveforms to be processed with a threshold retracker. To assess their performance, we also retracked the decontaminated and modified full-waveforms. The first meaningful sub-waveform and full-waveform in the original waveforms were retracked to compare the performance of the modified and decontaminated waveform retracking with the original waveform retracking. To compare the results of our sub-waveform retracking algorithms with those of external sub-waveform retracking algorithms, the (Adaptive Leading Edge Sub-waveform) ALES database was also used. In our retracking scenarios, we used the Sentinel-3A SRAL Altimeter to estimate the water levels over the study area within 10 km from the coastlines in both the Persian Gulf and the Bay of Biscay from June 2016 to October 2020. The water levels from processing L2 products were estimated as well. We evaluated our retracking scenarios and L2, as well as the ALES processing results, against the tide gauges. Our analysis showed that within 0–10 km from the coast, the first meaningful sub-waveform of the decontaminated waveforms had the best performance. We reached maximum RMS improvements in this scenario of 53% and 86% over the Persian Gulf and the Bay of Biscay, respectively, in comparison with L2 processing. Over these distances from the coast, the first sub-waveform from the original waveforms and the modified waveforms stayed in the second and third order of performance. The ALES database with an RMS ranging from 13 to 51 cm had a worse performance than all of our sub-waveform retracking scenarios.

Keywords: coastal altimetry; first sub-waveform; modified waveform; decontaminated waveform; original waveform

check for updates

Citation: Agar, P.; Roohi, S.; Voosoghi, B.; Amini, A.; Poreh, D. Sea Surface Height Estimation from Improved Modified, and Decontaminated Sub-Waveform Retracking Methods over Coastal Areas. *Remote Sens.* **2023**, *15*, 804. https://doi.org/10.3390/rs15030804

Academic Editor: Yi Luo

Received: 12 November 2022
Revised: 14 January 2023
Accepted: 19 January 2023
Published: 31 January 2023

Copyright: © 2023 by the authors. Licensee MDPI, Basel, Switzerland. This article is an open access article distributed under the terms and conditions of the Creative Commons Attribution (CC BY) license (https://creativecommons.org/licenses/by/4.0/).

1. Introduction

Coastal areas are commonly used to maneuver humans from land to oceans [1]. According to data from the CIESIN (Center for International Earth Science Information

Network), 39% of the world's population lives within 100 km of coasts [2] which are vulnerable due to floods, the erosion of agricultural areas, the destruction of infrastructure, and the leakage of salty water into groundwater and rivers. The sea-level rise exacerbates these threats. Therefore, monitoring water level variations in coastal areas is necessary to provide reliable data for making correct decisions to reduce environmental threats [3,4].

Tide gauge networks have provided accurate water level variation information for more than a century [5,6]. However, tidal gauge networks have many restrictions in terms of their spatial/temporal coverage, the lack of a unified database, the lack of a reference datum, accessibility issues, installation challenges, and maintenance costs. Moreover, the measurements of tidal gauge networks may be affected by land subsidence, which reduces the quality of such data [1,7,8].

The extension of satellite radar altimetry in 1993, with accurate and repeatable measurements that are free from atmospheric conditions and provide global coverage, created a big evolution in measuring coastal water from space [1,8,9]. Satellite radar altimetry was designed for open-ocean water surface monitoring. During recent decades, due to progress in radar sensor and data processing methodologies, the application of radar altimetry has been extended to coastal monitoring [8–10]. In coastal areas, due to the presence of non-water bodies, such as small islands, rocks, vegetation canopies, and calm sea surfaces, small bays and ports inside the footprint of the radar-reflected pulses create waveforms that deviate from the expected ocean waveform model, i.e., the Brown model [11]. As waveforms are fundamental in range measurements, they need to be retracked to achieve qualified ranges over these areas [9,12,13]. The capability of synthetic aperture radar (SAR) in water level monitoring has increasingly extended the application of satellite radar altimetry to coastal zones. The SAR altimeter was carried by the CryoSat-2 platform for the first time in 2010; thereafter, in 2016 and 2021, it was implemented on Sentinel-3 and Sentinel-6 satellites, respectively. The altimeter sends bursts of pulses to the earth's surface; based on the Doppler and multi-look processes, they provide a promising along-track resolution for about 300 m, but the across-track resolution remains as it was for the older generation of altimeters. That means that despite advances in radar-sensor and data processing methodologies, monitoring coastal zones is still a challenge for the SAR altimeter, especially when satellites fly parallel and close to the coastlines, because the radar footprint in the across-track direction is large and there are reflections from non-water objects [14–16] and from the calm sea surfaces in small bays and ports. Therefore, retracking waveforms over these areas is necessary.

The offset center of gravity (OCOG) of the waveform retracking algorithm, defined by Wingham [17], usually provides initial values for other retracking algorithms. In 1995, Davis [18] defined a statistical-retracking algorithm, called the threshold algorithm, which uses the parameters estimated by the OCOG algorithm. An improved threshold algorithm was used to retrack meaningful sub-waveforms over the Taiwan coast to estimate gravity anomalies based on Geosat data. The threshold algorithm showed a better performance than the β-5 parameter algorithm [19]. The β-parameter algorithm was developed by Martin [20] to retrack waveform icesheets. A modified waveform of Envisat and Jason-2 was retracked with the threshold algorithm over four coastal areas in North America, showing a better result with respect to L2 products and the processing of the original waveforms [21]. Decontaminated waveform methodology was developed in [22] to improve the deficiency of the modified waveform. This method showed a better result than the those of modified waveforms retracked with the threshold algorithm. Roohi et al. (2019) studied the performance of different retracking scenarios over a few lakes with different sizes and shapes around the world in different climate zones. They showed that the first and mean sub-waveforms retracked with the threshold and SAMOSA-3 algorithms provided a more accurate water level determination compared to the L2 products and scenarios with full-waveform retracking [23]. In another study [7], a sub-waveform that provides the water level close to the water level from tide gauges was analyzed over Lake Vänern in Sweden based on the Sentinel-3 SRAL data. For 90% of the waveform, the first sub-

waveform retracked with the threshold retracker gave the most optimized result compared to other scenarios. In marginal seas in Southeast Asia, the water level variations from Sentinel-3 waveforms based on the improved threshold, SAMOSA+, and the meaningful sub-waveform was retracked with the threshold algorithm with an RMS of less than 20 cm for all the scenarios. The SAMOSA+ algorithm provided a better result with respect to the other two scenarios [14]. In Ref. [10], all the gates in each waveform with outlier powers were constructed using interpolation, the so-called decontamination method, and then retracked using the threshold and Ice-1 algorithms. They were also compared with the ALES and PISTACH products. At a distance of 0–4 km from the coast, the waveform decontamination method achieved a better result than the other scenarios. According to [24–26], the ALES retracker, which is based on the sub-waveform retracking, provides a reliable sea surface height near the coast; therefore, we also used this dataset to evaluate our sub-waveform retracking scenarios in front of the tide gauges.

According to Refs. [7,23], retracking the first meaningful sub-waveform has a better performance than that of the original full-waveform. It was also shown in Refs. [10,21,22] that the retracking of the modified and decontaminated full-waveforms had a better performance than the retracking of the original full-waveforms. However, in this study, our objective is to evaluate the performance of the first sub-waveform retracking in the modified, decontaminated, and in the original waveforms to find an optimized retracking scenario.

In coastal zones, the return waveforms may be multi-peaks due to reflections from non-water objects. This type of the waveform cannot be correctly retracked with conventional retracking algorithms. To estimate a correct/accurate water level from waveform retracking, the pseudo peaks need to be corrected. In this study, we compared the water level obtained from the first sub-waveform in the modified and the decontaminated waveforms, as well as in the original waveforms with the threshold retracker. Full-waveform retracking was also performed for the decontaminated, modified, and original waveforms. We applied our retracking methodology over 0–10 km areas off the coast of the Persian Gulf and the Bay of Biscay using Sentinel-3A SRAL L2 and L1b data. The results obtained from the satellite data were validated with the tide gauge data for both study areas.

2. Materials and Methods

2.1. Data and Study Areas

In this study, we analyzed L1B and L2 data from Sentinel-3A SRAL over the Persian Gulf and the Bay of Biscay at 10 km from the coast. We evaluated the results of our analysis with the tide gauge data for both areas.

2.1.1. Sentinel-3 SRAL Data

The Sentinel-3 mission is a part of the Copernicus program, which is operated and controlled by ESA and EUMETSAT. The first satellite in the Sentinel-3 series, Sentinel-3A, was launched on 16 February 2016. It carries the SRAL altimeter and SLSTR and OLCI optical sensors. The SRAL is an SAR altimeter operating in the C and Ku bands with a global coverage. An interesting characteristic of this altimeter is the higher pulse repetition frequency with the capability of multi-looking measurements, which provide more observations and consequently more accurate/precise products [27–29]. We used SRAL SR _1_ SAR and SR _2_ LAN data for the period from June 2016 to October 2020. Table 1 summarizes some characteristics of the Sentinel-3 mission.

Table 1. Characteristics of Sentinel-3A mission [27–29].

Characteristic.	Description	Characteristic	Description
Orbit Height (km)	814.5	Repeat cycle (day)	27
Bands (GHz)	Ku (13.6), C (5.4)	Along-track resolution (m)	300
Pulse length (ns)	3.125	PRF (KHz)	17.8
Number of waveform gates	128	Nominal gate	43

2.1.2. Tide Gauge Dataset

To evaluate the water level from the satellite, we used data from two tide gauge stations for each study area. The measurement rate of these data is 15 min in the Persian Gulf and 10 min in the Bay of Biscay. We have summarized the information from these two tide gauge stations in Table 2.

Table 2. Tide gauge stations information.

Coastal Zone	Pass	Tide Gauge	Latitude	Longitude	Data Duration	Direct Distance from Track Position (Km)
Persian Gulf	25	Bushehr	28°59′N	50°50′E	17 January 2018 18 May 2019	4
	139	Kangan	27°50′N	52°03′E	21 September 2018 27 September 2019	2
Bay of Biscay	216	ILE-D-AIX	46°0.42′N	1°10.44′W	16 April 2016 26 August 2020	3.5
	485	La-Rochelle	46°8.88′N	1°13.5′W	25 April 2016 12 July 2020	19

2.1.3. ALES Dataset

The ALES Sentinel-3A dataset is produced by DGFI-TUM (Deutsches Geodätisches Forschungsinstitut Technische Universität München) and distributed via the Open Altimeter Database (OpenADB, https://www.openadb.dgfi.tum.de, accessed on 10 January 2023). The ALES sea surface height is based on the ALES retracker, which is based on sub-waveform retracking. This adaptive retracker uses the significant wave height to model the sub-waveform based on the Brown model in a least square estimation procedure [10]. More details about the retracker and the products can be found in [24,30,31].

2.1.4. Persian Gulf

The Persian Gulf, with an area of 251,000 km^2 and an average depth of 30 m, is a semi-enclosed body of water connected to the Arabian Sea by the Strait of Hormuz and the Sea of Oman. This relatively large body of water is located in a subtropical and arid climate zone with temperature fluctuations from 0 °C in winter to 50 °C in summer. This range of temperature fluctuations leads to fluctuations in the water level. Because of its gas and oil deposits, the Persian Gulf is a very important area politically, militarily, and economically. It is also one of the busiest waterways in the world [32,33].

2.1.5. Bay of Biscay

With an area of 175,000 km^2, the Bay of Biscay is located in the middle of the northeastern Atlantic Ocean between France and Spain. In this area, the continental shelf is narrower in the south than in the north. Ocean circulations are induced by stronger tidal influences, seasonal wind regimes, whirlpools, and river runoff. The tidal currents in this area are strong, making it an ideal dynamic study area for study and research [34]. Figures 1 and 2 show the locations of satellite-selected passes and tide gauge stations for the Persian Gulf and the Bay of Biscay, respectively.

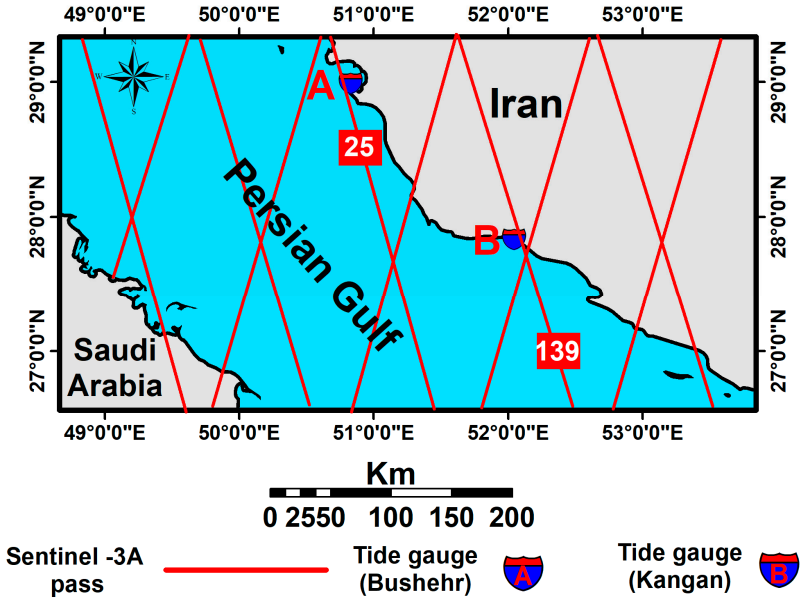


Figure 1. The location of the Sentinel-3A ground passes and tide gauge stations A (Bushehr) and B (Kangan) in the Persian Gulf.

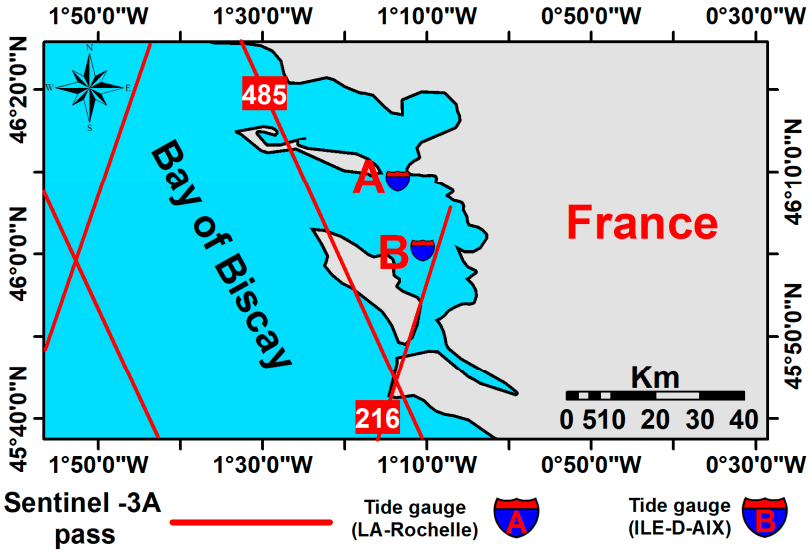


Figure 2. The location of the Sentinel-3A ground passes and tide gauge stations A (La-Rochelle) and B (ILE-D-AIX) in the Bay of Biscay.

2.2. Principles of Satellite Radar Altimetry

An altimeter sends continuous electromagnetic pulses with limited known power toward the earth's surface and then a part of the pulses reflected from the surface at a specific interval time (known as bin or gate) figure out the waveforms. Based on the round-trip travel time, Δt of the pulse, the range between the satellite and the surface can be calculated as follows:

$$R = \frac{1}{2} \times C \times \Delta t \quad (1)$$

in which C is the speed of light [35].

The waveforms are progressively representative of the powers of the pulses reflected from the surface [8]. Over oceans, where the reflecting surface is usually homogeneous (water only), the waveform shapes are simple and usually follow the Brown model [11]. In such a model of the waveform, a gate located in the middle of the leading edge, so-called the nominal gate, is a reference for measuring the round-trip travel time, i.e., the

delay [9]. However, in the presence of calm water surfaces such as small bays/ports inside the footprint, there would be strong reflections that would corrupt the waveforms. For the corrupted waveforms, this nominal gate is not a correct reference in delay measurements. Therefore, the returned waveforms must be post-processed/retracked to derive a correct gate, i.e., a retracked gate, for the delay measurements [9,13,36]. Figure 3 shows a few examples of the waveforms over the Persian Gulf at a distance of 0 to 10 km from the coasts.

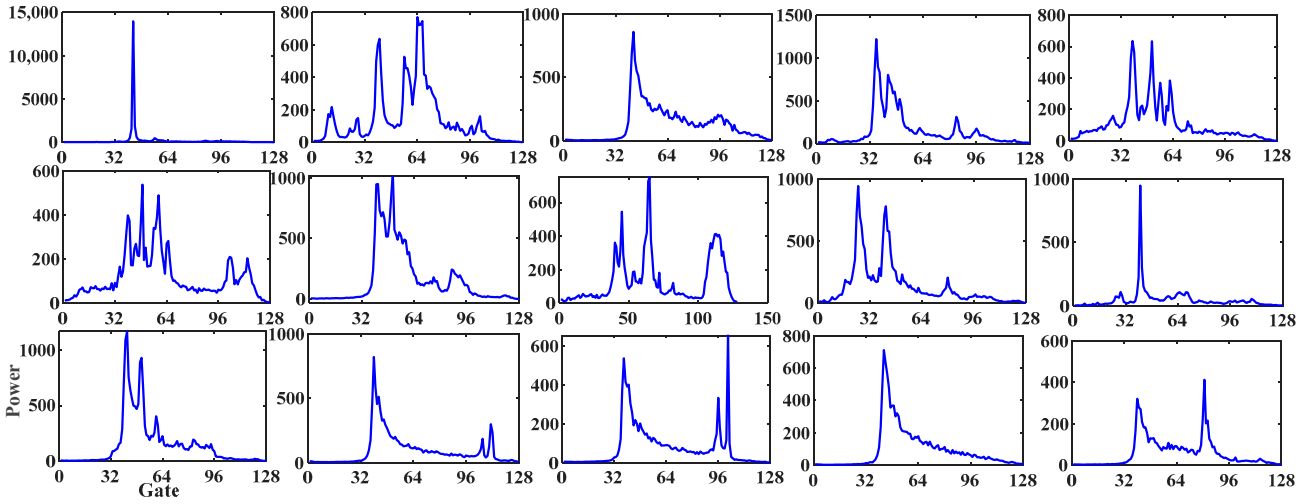


Figure 3. Example of waveforms from pass 25 over the Persian Gulf at 10 km from the coast.

The retracked correction (C_{ret}) is calculated from [37]:

$$C_r = (G_r - G_0) \times \frac{C}{2} \times \tau \quad (2)$$

in which G_r is the retracked gate and G_0 is the nominal gate, C is the speed of light, and τ is the gate width. This retracked correction plus media (C_{media}) and geophysical ($C_{geophysical}$) corrections are added to the ranges to estimate the water level variations [38,39]:

$$SSH = H - (R + C_{ret} + \sum C_{media} + \sum C_{geophysical}) \quad (3)$$

$$\sum C_{media} + \sum C_{geophysical} = C_{iono} + C_{dry\ tropospheric} + C_{wet\ tropospheroc} + C_{SSB} + C_{tides} + C_{DAC} \quad (4)$$

In Equation (4), C_{iono} is the ionospheric, C_{dry} is the dry atmospheric, C_{wet} is the wet atmospheric, C_{SSB} is the sea state bias, C_{tide} is the tidal, and C_{DAC} is the dynamic atmospheric correction.

2.3. Waveform Retracking Scenarios in This Study

Waveforms vary in coastal areas due to the shape of shorelines, the water depth, possible rocks, vegetation cover, and climate conditions. So, it would be very difficult to find a unified retracking algorithm that performs precisely/accurately in any coastal area. According to the previous studies as mentioned in the introduction, e.g., [18], the threshold retracker has a better performance than other retrackers in coastal areas. Therefore, we implemented this retracker with different thresholds to retrack the waveforms in different scenarios. These waveform retracking scenarios are explained below.

2.3.1. Retracking the Full Original Waveforms

In this scenario, a given waveform is considered as one waveform, the so-called full-waveform, and it is retracked. Figure 4a shows a simple ocean-like full-waveform in which the nominal and retracked gates are identical. Figure 4b, however, represents a corrupted multi-peak waveform.

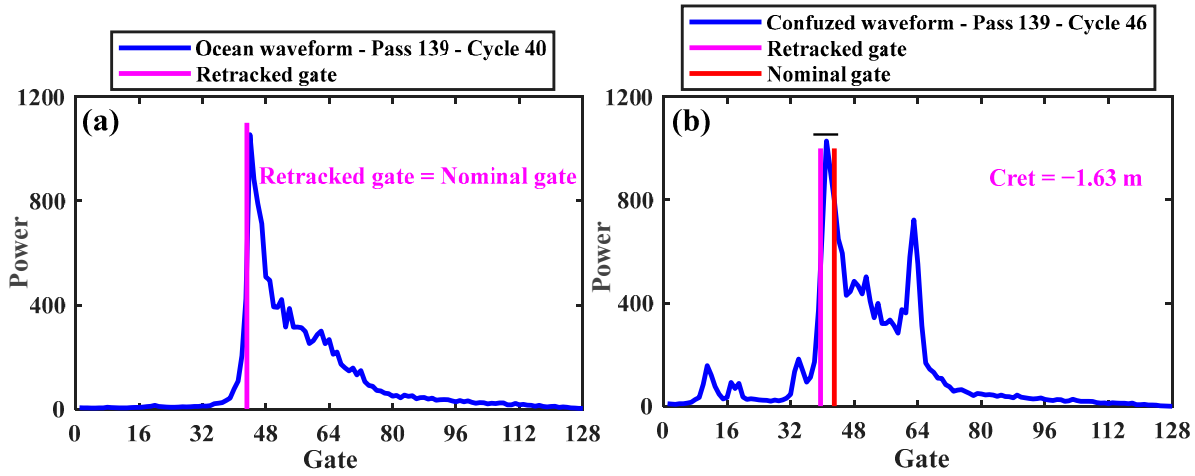


Figure 4. Retracking the full original waveform using threshold retracker with 30% threshold for pass 139 over Persian Gulf; (**a**) is an ocean-like and (**b**) is a corrupted waveform.

2.3.2. Retracking the First Sub-Waveform in the Original Waveforms

Waveforms in coastal areas are usually multi-peaks. Each meaningful peak can be considered as a small waveform, called a sub-waveform. The meaningful sub-waveform is detected and retracked [40]. We assume that the first peak is the response from the water surface and that it is the right sub-waveform to be retracked. We implemented the methodology described in [19] to identify the meaningful sub-waveforms. Figure 5a,b show a multi-peak waveform of the 216 and 485 passes over the Bay of Biscay. In this figure, S and E stand for the start and end of the leading edge, respectively, in each meaningful sub-waveform.

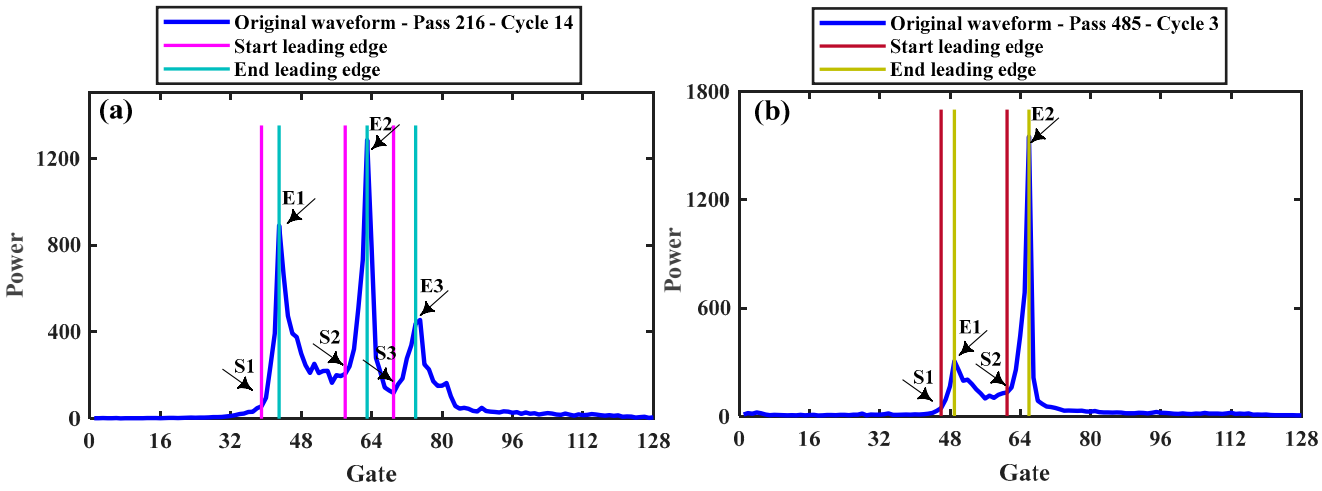


Figure 5. Meaningful detected sub-waveforms in (**a**) pass 485 cycle 3 and (**b**) pass 216 cycle 14 over the Bay of Biscay.

According to the previous studies [7,23,41,42], the first sub-waveform retracking outperforms the other sub-waveform retracking scenarios, so we have considered only the first sub-waveforms. Figure 6 shows the retracked gates from the full-waveform (magenta) and the first sub-waveform (cyan) of pass 25 over the Persian Gulf. In this figure, OriW stands for the original waveform, DW for the decontaminated waveforms, and MW for the modified waveforms.

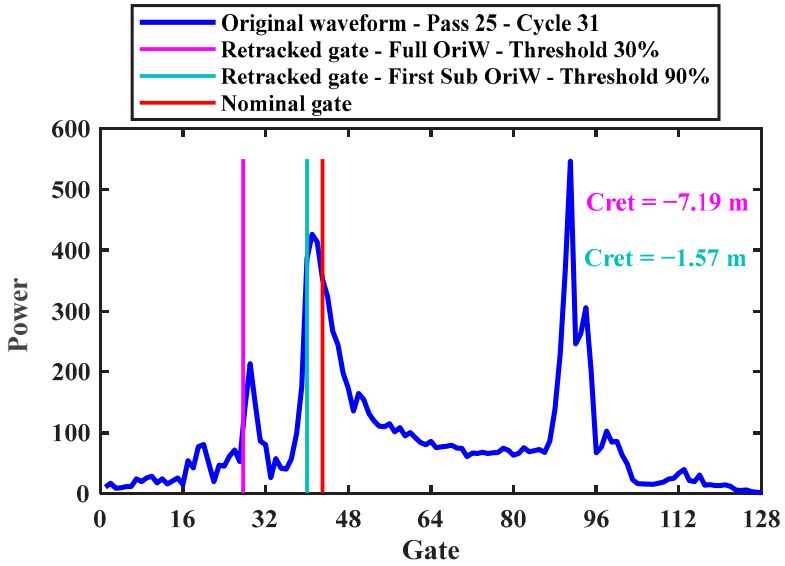


Figure 6. Retracked gates obtained from the full-waveform and the first sub-waveform of pass 25 cycle 31 over the Persian Gulf.

2.3.3. Retracking the Modified Full-Waveforms

Waveforms in coastal areas usually have outlier powers in some gates. In order to find the correct retracked gate, the outlier powers need to be corrected statistically, which leads to modifying the waveforms [21]. In this modification, one needs to define a reference waveform (P_{ref} (i)). It is constructed by averaging the waveforms from 20 to 30 km of coastline for each satellite overpass in each cycle, since the state of the water surface varies from cycle to cycle. Based on this reference waveform, the outlier powers are determined from the following constraint:

$$\text{if} |P_C(i) - P_{ref}(i)| > 2\sigma \Rightarrow P_C(i) = P_C(\text{out}) \tag{5}$$

in which P_C (i) is the power of the ith gate in the Cth waveform and σ is the standard of the power difference between the reference and original waveforms. The outlier powers are corrected by linear interpolation based on the powers of the neighboring gates in the same waveform and the nearby gates in the adjacent waveforms.

$$\begin{aligned} \overline{P}_C(i) = \tfrac{1}{2\sqrt{2}+4}\{[P_C(i+1) + P_C(i-1) + P_{C+1}(i) + P_{C-1}(i)] + \ldots \\ \tfrac{1}{\sqrt{2}}[P_{C+1}(i+1) + P_{C-1}(i-1) + P_{C+1}(i-1) + P_{C-1}(i+1)]\Big\} \end{aligned} \tag{6}$$

In this equation, $\overline{P}_C(i)$ is the replacing power for the outlier power in the ith gate and the Cth waveform. The $P_{C\text{-}1}$(i) and P_{C+1}(i) are the powers from the adjacent waveforms [21].

Figure 7 shows the modification of a given waveform in pass 25 of cycle 34 over the Persian Gulf. In this figure, the outlier boundaries are marked with pink lines of ±2σ. The powers outside the boundaries are considered as outliers which are marked with solid red circles.

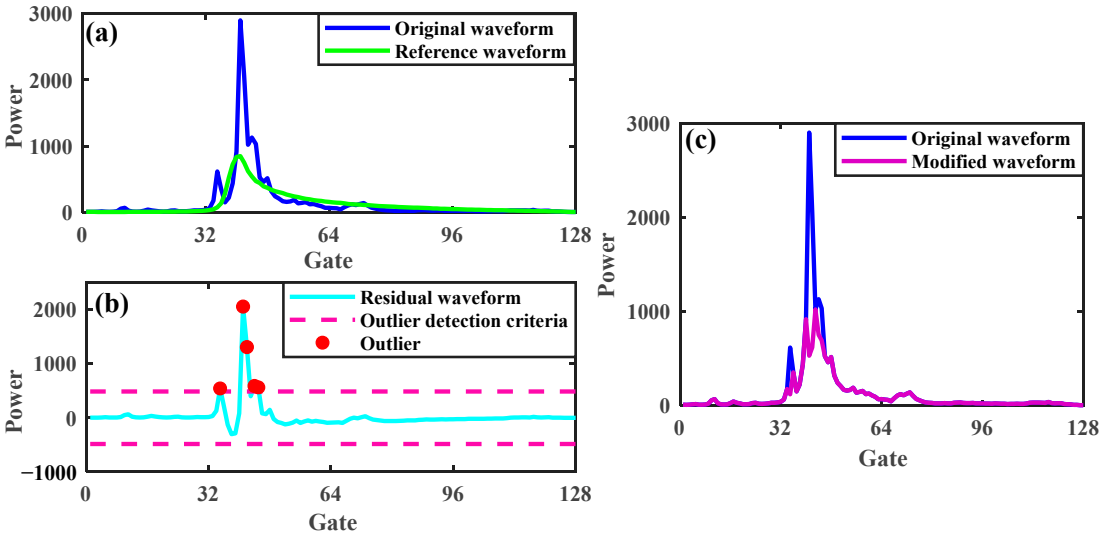


Figure 7. Waveform modification for a waveform in pass 25 of cycle 34 in the Persian Gulf (**a**) is the original waveform, (**b**) is the detected outlier powers, and (**c**) is the modified waveform.

After the modification, they were retracked with the threshold retracker to derive the retracked correction. Figure 8 shows the original waveform in blue and the modified waveform in magenta. As can be seen from this figure, there is an unusual power in gate 64 which leads to a completely different retracked range correction if it is not modified. If the unusual peak is considered a true peak and used for the retracked correction, we come up with a 9.38 m range correction, while with the modification, the retracked range correction is 1.31 m.

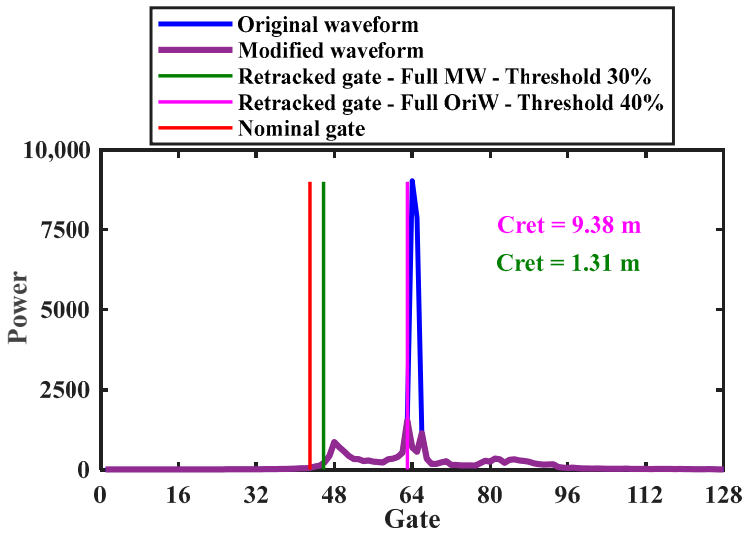


Figure 8. Retracked the original and modified waveform of a given waveform in pass 25 cycle 44 in the Persian Gulf.

2.3.4. Retracking the Decontaminated Full-Waveforms

The procedure for finding outliers in the waveforms with changes in the criteria is similar to the modification strategy. In this strategy, a reference waveform is defined at 0–20 km from the coast. It is expected that the reference waveform (due to the presence of the coastal waveform in the definition of the reference waveform) has a better match with the coastal waveform. The criterion for detecting outliers is the RMS defined in Equation (7). In the modification strategy, the retrieved and refined outlier powers depend on the interpolation process. If the neighboring gates in the same waveform and the neighboring gates in the adjacent waveforms around the detected outlier have powers

slightly smaller than the outliers and are not detected as outliers, the interpolation process is not performed correctly. As a result, the retracked gate would not be correctly determined, which leads to an erroneous range measurement. Therefore, it is better to exclude the outlier powers in determining the retracked correction instead of being corrected through interpolation. This is the main point of retracking the decontaminated waveforms.

$$\mathrm{RMS} = \sqrt{\frac{\sum_{n=1}^{N}\sum_{i=1}^{M}\Delta P_n^2(i)}{NM}} \quad i = 1, 2, ..., 128 \tag{7}$$

In this equation, N is the total number of waveforms and M is the number of gates in the waveform and $\Delta P_n(i)$ is the power difference of the ith gate in the reference waveform and the ith gate of the nth waveform in the coastal waveform [22]. The green and red waveforms shown in Figure 9a are the reference waveforms for the decontaminated and modified waveforms, respectively. The blue color represents the original waveform. The difference between the reference waveform from the modification strategy and the original waveforms leads to incorrectly detected outliers. The wrongly detected outliers are marked in cyan on Figure 9b. However, with the decontaminated waveform strategy, this problem does not exist anymore because the reference waveform is closer (more similar) to the original waveform than with the modification strategy. In this figure, two parallel straight lines of $\pm 2\sigma$ and $\pm$RMS in magenta and orange represent the outlier boundary detection for the modified and decontamination strategies, respectively.

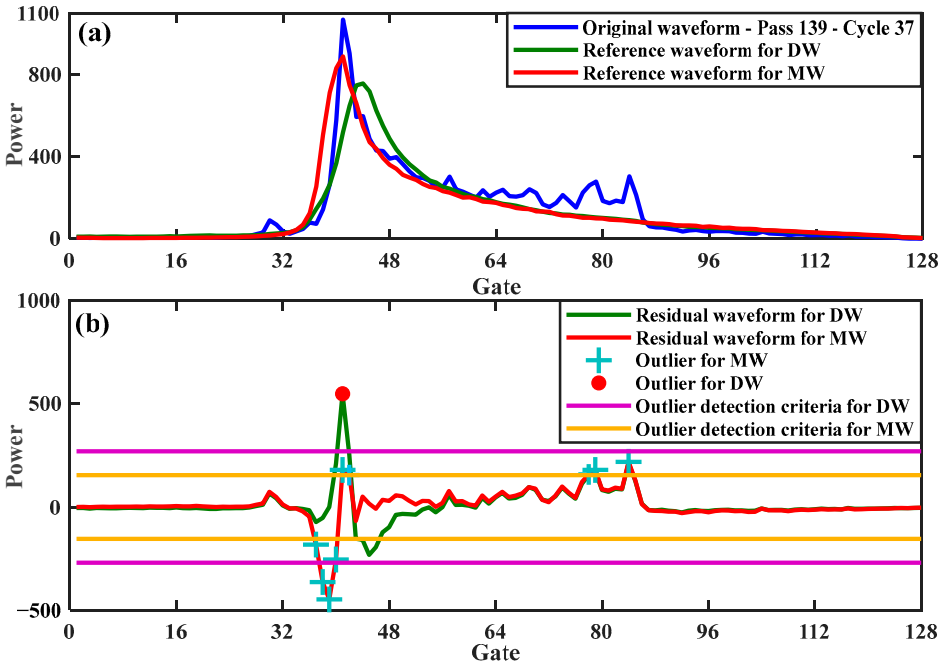


Figure 9. Fitting the reference waveforms (**a**) and detection of outliers (**b**) in a particular waveform of pass 139 and cycle 37 over the Persian Gulf using the modification and decontamination strategies.

The decontaminated waveforms were then retracked using the threshold retracker to evaluate the performance of this strategy.

Figure 10a shows the original and the reference waveform with the detected outlier. Figure 10b shows the location of the retracked gates for the original and decontaminated waveforms from the threshold retracker. As one sees from the figure, the exclusion of the gates with outlier powers leads to finding the retracked gate in the steeped leading edge part of the waveform, which is usually expected.

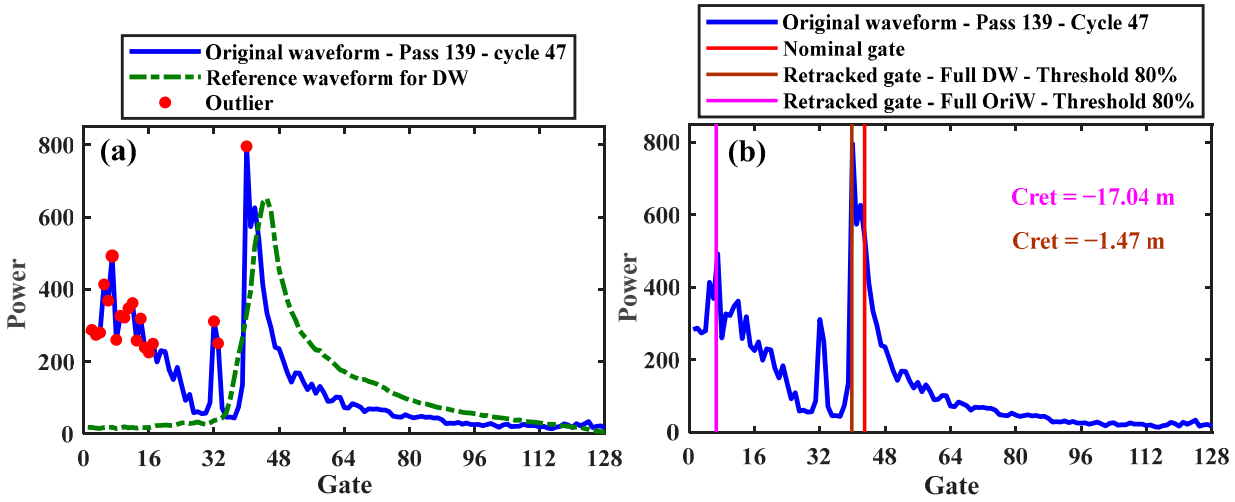


Figure 10. (**a**) Reference and original waveforms with detected outliers for a waveform of pass 139 in cycle 47 over the Persian Gulf, (**b**) retracked gates/corrections of the decontaminated and original waveform derived from the threshold retracker.

2.3.5. Retracking the First Sub-Waveform in the Decontaminated Waveforms

In this retracking strategy, the coastal waveforms were first decontaminated as described in Section 2.3.4, then the first meaningful sub-waveforms were detected and retracked using the threshold retracker. Since outliers were filtered out from the first meaning sub-waveform, the retracked gates were estimated more accurately than those from the first sub-waveform in the original and modified waveforms. Figure 11 shows a waveform of pass 216 from cycle 56 (over the Bay of Biscay) that was retracked based on this strategy, with the position of the retracked gate shown in green. The location of the retracked gate for the first sub-waveform of the original waveform is marked with cyan and the nominal gate with red. The retracked correction of the original waveform is 2.65 m, while this correction of the decontaminated waveform is 2.09 m.

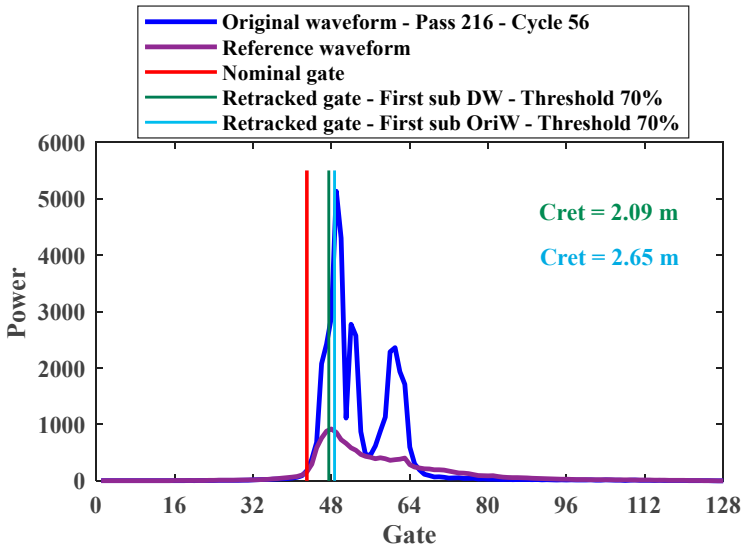


Figure 11. Retracking of the first sub-waveform of the original and decontaminated waveform of pass 216 from cycle 56 over the Bay of Biscay.

2.3.6. Retracking the First Sub-Waveform in the Modified Waveforms

In this scenario, the modification was first performed as described in Section 2.3.3. The modified waveforms were then scrutinized to find the first meaningful sub-waveform

that could be retracked with the threshold retracker. Figure 12 shows an example of such a retracking scenario.

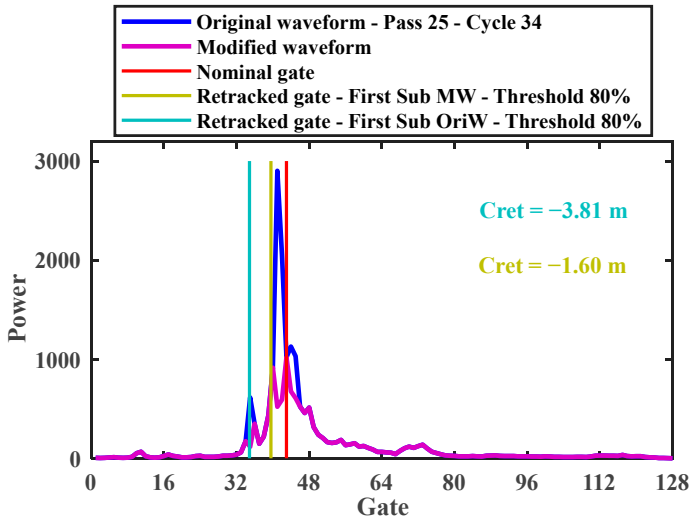


Figure 12. Retracking of the first sub-waveform of the original and modified waveform of pass 25 and cycle 34 over the Persian Gulf.

2.4. Water Level Estimation and Validation

In this section, we describe the steps to determine the water level. We derived the water level variations from the satellite data according to the following steps [23]:

1. Instantaneous water level estimation

The water level variations for each satellite overpass have been derived based on Equation (3) for Sentinel-3 level 2 and level 1-B (retracking scenarios) data.

2. Detecting and removing outliers

Possible outliers of the instantaneous water level have been removed based on the mean water level at a confidence level of 95%. Figure 13 shows an example of this processing step.

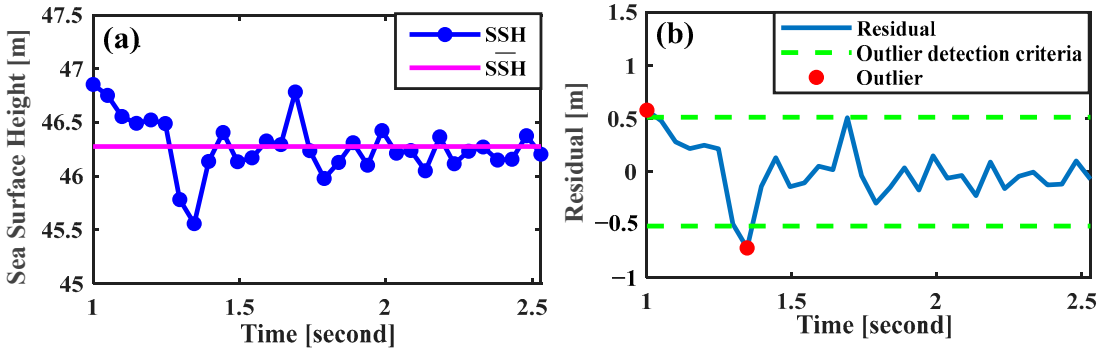


Figure 13. (**a**) The instantaneous (blue) and mean (magenta) water level of the Bay of Biscay from track 485 and cycle 39 as well as (**b**) outliers' rejection.

3. Water level time series for each pass

The median water level of all the instantaneous water level time series was merged to build a long time series for each pass covering the entire period of the study. The median value of the water level is independent of the very small or large values, so it provides a more precise water level. For this reason, we used the median and not the mean or all values of the instantaneous water level. The performance of the median values was demonstrated in [40].

4. Elimination of possible bias between satellite water level time series and tide gauge data

The satellite-derived water level was validated against the tide gauge data. Generally, the tide gauge data follow a national policy and may have a local or national reference datum which is different from the satellite datum. To evaluate the satellite-derived water level, the possible bias should be removed before comparing the two-time series. The RMSE between the satellite and tide gauge time series is a criterion for evaluating the performance of each retracking scenario.

3. Results and Discussion

3.1. Water Level from L2 Products

Numerical and graphical results of water level variation derived from processing L2 products (level 2) and different retracking scenarios are discussed in this section. Table 3 includes validated results obtained from processing L2 products in terms of the RMSE with respect to the tide gauge data. The more precise results are indicated by underlined numbers.

Table 3. RMSE values (cm) of water level variations derived from L2 products compared to the tide gauge data.

Pass/Retracker	OCOG	Ocean	Ice Sheet	Sea Ice	Tracker
25	32	39	37	57	40
139	12	14	12	28	75
216	116	148	89	194	210
485	9	9	9	20	144

As shown in Table 3, processing L2 products with an RMS greater than 30 cm (with respect to the tide gauge data) did not provide a qualified water level variation for passes 25 and 216. Pass 216, with an RMS of over 80 cm, provides the most unqualified result of the water level determination. As can be seen in Figure 2, during this pass, the satellite flies close to and parallel to the coastline, where the existence of non-water objects is more probable. It deviates the waveform's shape from the expected one, i.e., the Brown model, and consequently leads to very high RMS values. However, L2 processing provided a qualified water level for passes 139 and 485. As shown in Figure 1, the orientation of the satellite passes with respect to the shoreline is such that the satellite does not face obstacles (non-water objects) in illuminating the water surface. Therefore, the waveforms are not corrupted much (Figure 14) and the L2 products provide a qualified water level. We have randomly plotted a few waveforms of this pass to represent that the waveforms are mostly healthy or less corrupted.

A comparison of the results presented in Table 3 shows that the L2 products are not able to provide qualified water level variations for all passes, which signifies the necessity of retracking in coastal areas.

3.2. Water Level from Our Retracking Scenarios

In Tables 4–7, the result of the water level determination from our retracking scenarios based on the threshold retracker with different threshold values is provided. The more precise results are indicated by underlined numbers.

Table 4. RMSEs (cm) of the water level from retracking the first sub-waveform and the full-waveform in the original waveforms (RMSE: first sub-original waveform/original full-waveform).

Pass/Threshold	10%	20%	30%	40%	50%	60%	70%	80%	90%
25	21/54	21/31	20/26	20/28	20/29	20/31	19/32	19/32	18/32
139	15/288	14/56	13/38	14/14	13/13	13/12	12/12	12/12	11/12
216	24/36	23/33	21/54	20/64	18/61	18/75	17/109	16/122	18/122
485	10/10	9/10	9/9	9/9	9/9	9/9	9/9	9/9	10/9

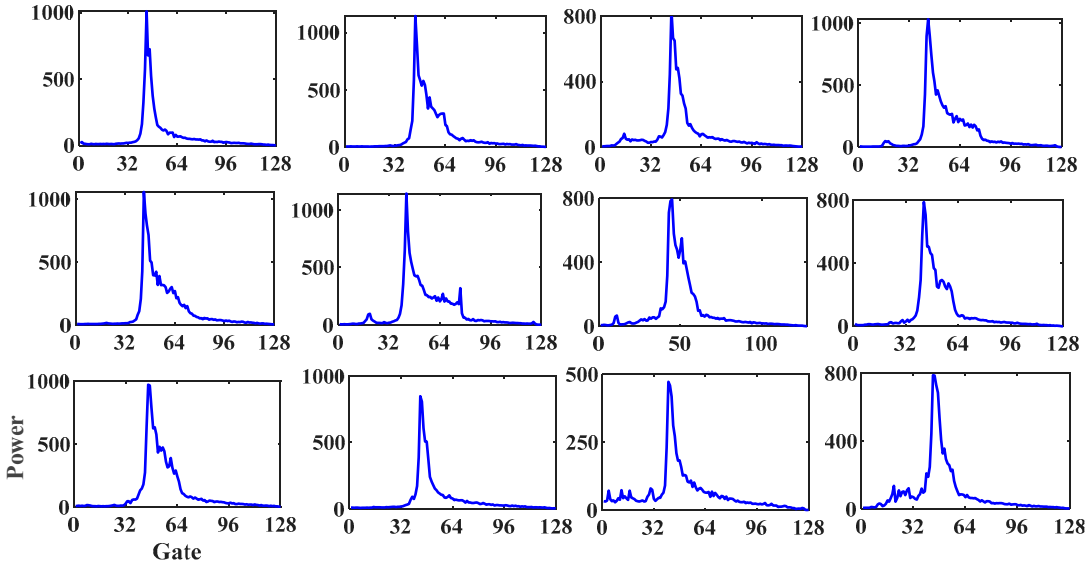


Figure 14. Example of waveforms from pass 139 over the Persian Gulf at 0 to 10 km from the coast.

Table 5. Waveform statistical information.

Pass	Total Number of Waveforms	Multi-Peak	Percentage (%)
25	982	629	64
139	391	58	15
216	1955	954	49
485	2279	518	23

Table 6. RMSEs (cm) of the water level from retracking the full-waveform of decontaminated/modified waveforms (RMSE: decontaminated full-waveform/modified full-waveform).

Pass/Threshold	10%	20%	30%	40%	50%	60%	70%	80%	90%
25	57/44	23/44	25/33	29/21	30/24	28/29	30/33	34/34	40/33
139	-/299	-/116	-/40	14/14	13/15	13/14	11/15	11/13	11/14
216	29/27	46/25	53/27	75/34	106/37	124/51	144/67	148/88	178/110
485	10/38	9/25	9/20	9/18	8/16	8/11	8/9	8/9	9/10

Table 7. RMSEs (cm) of the water level from retracking the first sub-waveforms in decontaminated/modified waveforms (RMSE: first sub-decontaminated waveform/first sub-modified waveform).

Pass/Threshold	10%	20%	30%	40%	50%	60%	70%	80%	90%
25	20/14	17/14	16/15	15/19	18/19	19/16	19/12	19/11	18/11
139	15/21	15/15	14/17	14/16	13/14	12/14	11/14	10/15	11/14
216	21/25	19/23	16/22	14/20	13/20	15/20	12/19	14/19	17/20
485	9/14	9/15	9/12	9/10	8/10	8/11	8/12	9/14	10/17

As can be clearly seen from Table 4, the first sub-waveform retracking provides better results than the full-waveform retracking. In pass 485, there is the same performance for the first sub-waveform and the full-waveform retracking because, as shown in Table 5, about 80% of the waveforms in this pass have a simple shape. Thus, the full-waveform retracking has a very good performance too. Where the waveforms are multi-peaks, the first sub-waveform retracking is showing a promising result. For example, in pass 216, 49% of the waveforms are multi-peaks, so the sub-waveform has a better performance. Pass 25 with 64% multi-peak waveforms has the same story as pass 216.

As shown in Table 6, there is generally not a clear distinguish between the performance of the modified and decontaminated waveforms when we consider the full-waveform retracking in terms of the water level RMSE values.

The numerical result in Table 7 shows that retracking the first sub-waveform in the decontaminated waveforms leads to a better result than the modified waveforms in three out of four passes. Near the coast, the waveforms are more corrupted; therefore, the reference waveform of the modified waveforms cannot be fit to the original waveforms to detect outlier powers. Therefore, the outlier powers are not correctly modified which leads to higher RMSE values in the retracking of the modified waveforms. However, this issue is not significant for retracking the first sub-waveform in the decontaminated waveforms because all waveforms within 10 km of the coast are involved in the definition of the reference waveform. Therefore, the reference waveform has a better match to the original waveforms to detect and remove outlier powers.

Table 8 provides a summary and overview of all our retracking scenarios, the ALES retracker, and L2 processing. It also shows the percentage of improvements (IMPs) by our methodology and by the ALES with respect to the L2 products and the percentage of accepted measurements in all cycles (the more precise results and the maximum IMPs are indicated by underlined numbers in Table 8). From this table, one sees that the first sub-waveform retracking in the decontaminated waveforms has a better performance in determining the water level. The alternative scenarios are the first sub-waveform in the original and modified waveforms. According to this table, our sub-waveform retrackings outperform the ALES retracker. We used the threshold retracker as recommended by previous studies in the coastal areas to retrack the sub-waveform. However, the ALES retracker is based on the Brown model, which has a better performance over the open ocean.

According to this table, the performance of retracking the modified and decontaminated waveforms is slightly better than that of the original waveforms in the case of retracking the full-waveform. However, these scenarios require a lot of processing (they are slow) to provide water level variations and, finally, there is no significant difference between the result. Over 10 km patches, there is no significant difference between the modified and decontaminated waveform retracking based on full-waveform retracking.

Our numerical result in Table 8 also shows that the sub-waveform retracking scenarios based on the threshold algorithm generally perform better than the full-waveform retracking scenarios, which is in line with the results of previous studies, e.g., [23]. Sub-waveform retracking is effective over challenging areas, small lakes, narrow rivers, and near the coast. Near coasts, waveforms are usually multi-peaks and conventional retracking algorithms are not able to provide a correct/precise retracking correction. However, over areas farther from the coasts (more than 10 km), the reflecting surface within the radar footprint is homogeneous, i.e., purely water. Therefore, the returned waveforms are close/similar to the expected model, the Brown model, which can be well retracked by conventional retracking algorithms. In these areas, there is no significant difference between the performance of sub-waveform and full-waveform retracking scenarios.

An intercomparison of sub-waveform retracking scenarios shows that the retracking of the first sub-waveform in the decontaminated waveforms has a better performance than the others. The first sub-waveform retracking in the original waveforms also has a good performance. Defining the reference waveform where they are multi-peaks is difficult for decontaminated and modified waveforms, which may affect their performance. However, retracking the first sub-waveforms in the original waveforms is independent of the reference waveform and the processing steps are less than those of the decontaminated and modified waveforms, i.e., it is faster.

The following Figures 15–18 show the result of some optimized retracking scenarios over 10 km patches.

Table 8. Performance evaluation of our retacking scenarios against ALES dataset and L2 product in front of tide gauge in terms of RMSE (cm) and IMP (%). It also includes the percentage of accepted measurements in all cycles (valid data).

Pass/Retracker		L2	ALES	Original Full-Waveform	Modified Full-Waveform	Decontaminated Full-Waveform	First Sub-Waveform in Original Waveform	First Sub-Waveform in Modified Waveform	First Sub-Waveform in Decontaminated Waveform
25	RMSE (cm)	32	25	26	21	23	18	11	15
	IMP (%)	-	22	19	34	28	44	66	53
	Valid data (%)	94	95	92	93	93	92	93	92
139	RMSE (cm)	12	20	12	13	11	11	14	10
	IMP (%)	-	-	-	-	8	8	-	17
	Valid data (%)	95	79	95	94	95	94	94	95
216	RMSE (cm)	89	51	33	25	29	16	19	12
	IMP (%)	-	43	63	72	67	82	79	86
	Valid data (%)	95	87	93	94	93	93	93	93
485	RMSE (cm)	9	13	9	9	8	9	10	8
	IMP (%)	-	-	-	-	11	-	-	11
	Valid data (%)	94	100	94	95	94	93	95	94

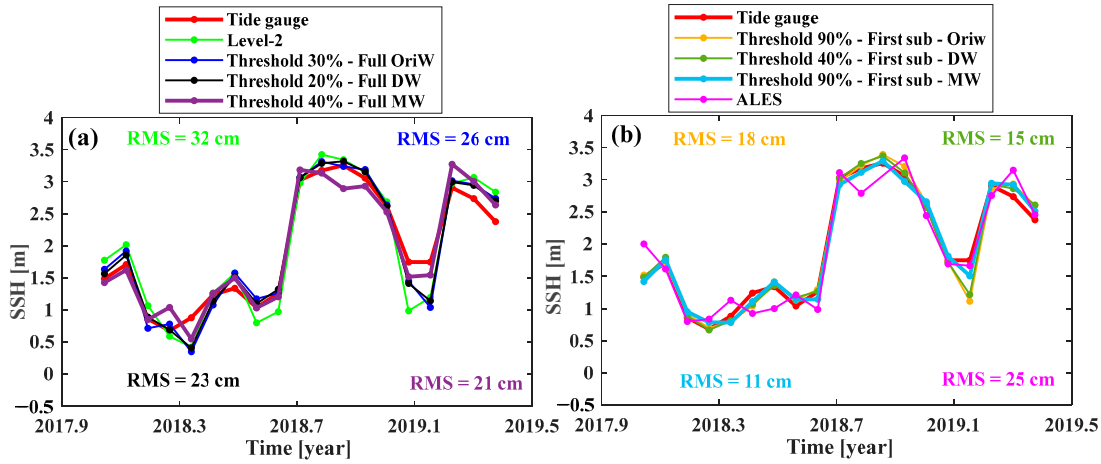


Figure 15. Water level time series of the Persian Gulf pass 25 based on our waveform retracking scenarios and ALES dataset in front of tide gauges, (**a**): full-waveform and (**b**): sub-waveform.

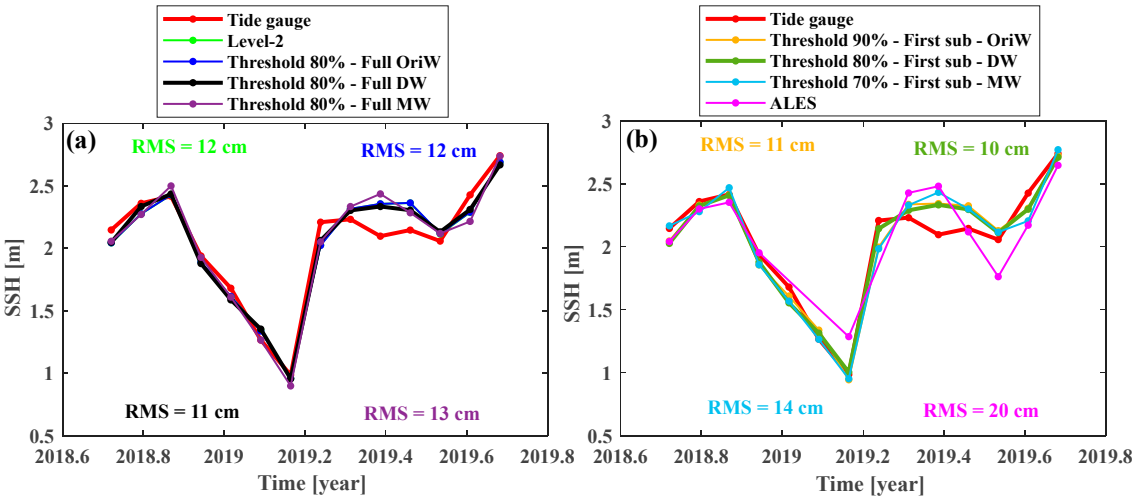


Figure 16. Water level time series of the Persian Gulf pass 139 based on our waveform retracking scenarios and ALES dataset in front of tide gauges, (**a**): full-waveform and (**b**): sub-waveform.

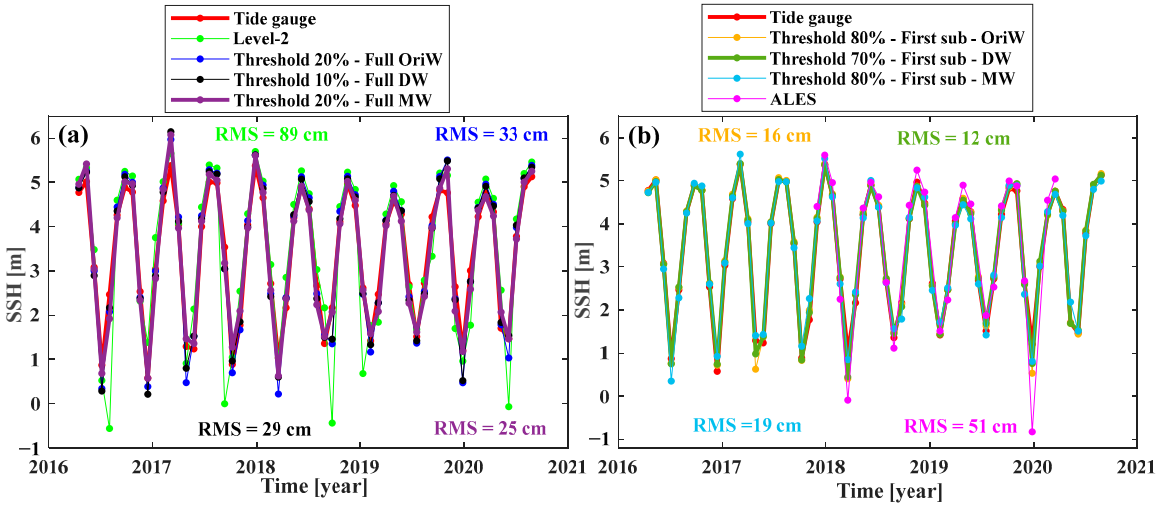


Figure 17. Water level time series of the Bay of Biscay pass 216 based on our waveform retracking scenarios and ALES dataset in front of tide gauges, (**a**): full-waveform and (**b**): sub-waveform.

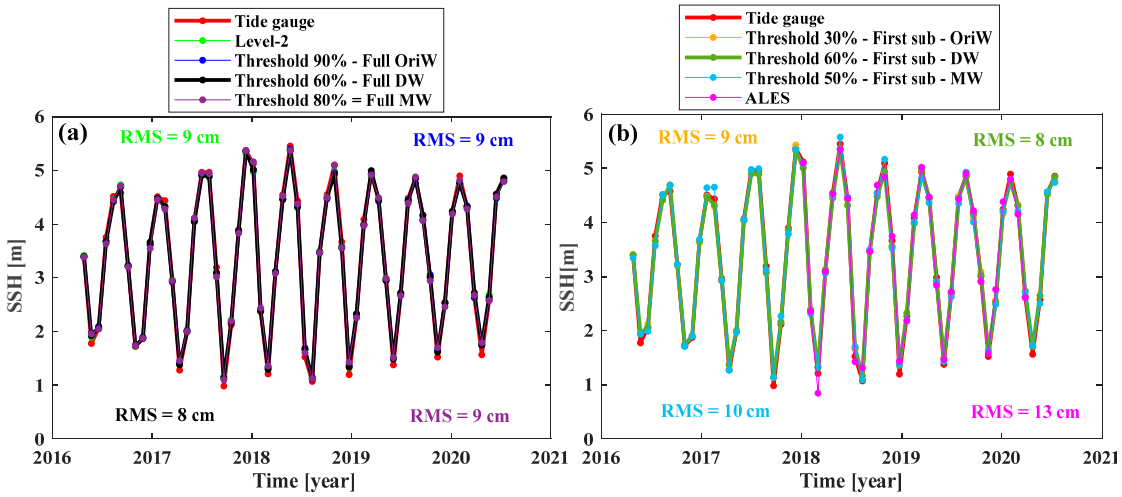


Figure 18. Water level time series of the Bay of Biscay pass 485 based on our waveform retracking scenarios and ALES dataset in front of tide gauges, (**a**): full-waveform and (**b**): sub-waveform.

4. Conclusions

In this study, we used data from the Sentinel-3A mission to estimate water level variations in the Persian Gulf (passes 25 and 139) and Bay of Biscay (passes 216 and 485) from June 2016 to October 2020 over 10 km patches from the coast. We analyzed the SRAL L2 and L1B products and evaluated the result against the tide gauge data corresponding to this time frame. Typically, altimeters are challenging when monitoring water levels in coastal areas because radar footprints are large enough to illuminate not only the water surface but also partially non-water surfaces. Reflections from the non-water surfaces and from the calm water surface (in small bays and ports) corrupt the return waveforms, which leads to an erroneous water level determination. New altimetry missions such as Sentinel-3 use the SAR mode for measurements and the SAR data processing methodology which decreases the size of the footprint by about 300 m in the along-track direction. However, the size of the footprint in the across-track direction remains the same as conventional altimeters, which still makes coastal areas a challenge for accurate/precise monitoring. This emphasizes the waveform retracking in these areas. To obtain a qualified water level for each study area, in addition to processing L2 products, we retracked waveforms included in the L1B products using the threshold retracker algorithm. We also used the ALES dataset to evaluate our waveform retracking scenarios.

We have considered different waveform retracking scenarios, including the full-waveform (original, modified, and decontaminated waveforms) and the sub-waveform, i.e., the first sub-waveform in the original, modified, and decontaminated waveforms. The performance of the L2 products and each of our retracking scenarios have been evaluated against the tide gauge data in the form of RMSEs. The capability of the retracking scenarios in determining the water level has also been determined in terms of a percentage improvement compared to the L2 products. Our findings in this study are:

- In coastal areas, waveform retracking is necessary to achieve a qualified determination of the water level;
- In these areas, the approaches of retracking the first sub-waveform in the decontaminated waveform, the modified waveform, and in the original waveform generally outperform the full-waveform retracking. This is in agreement with previous studies;
- Retracking the first sub-waveform in the decontaminated waveforms outperforms the first sub-waveform retracking in the modified waveforms because in the decontamination scenario, all waveforms within 10 km of the coast are involved in the definition of the reference waveform. So, the reference waveform fits better to the waveforms to detect and remove the outlier powers. Therefore, the outlier powers are correctly detected and, consequently, an accurate retracked correction is estimated which leads

to an accurate determination of the water level. However, in the modified waveform, the reference waveform is defined outside the study areas (20–30 km from the coast), so the reference is defined independently of the tested waveforms. Therefore, the reference waveform does not fit well to the waveform to detect and modify the outlier powers;

- Our sub-waveform retracking scenarios outperform the ALES because it is based on the Brown model. The Brown model is defined for waveforms over the open ocean. However, in the coastal areas, the threshold retracker has a better performance in the retracking process. This has been approved by previous studies, e.g., in [12,43,44];
- Decontaminated and modified scenarios in full-waveform retracking have a slightly better performance than full-waveform retracking in the original waveform;
- Based on our numerical results for both study areas, the optimized retracking scenario is retracking the first sub-waveform in the decontaminated waveforms. As an alternative, we recommend retracking the first sub-waveform in the original and then modified waveform. This is in line with our objective in this study.

Certainly, implementing our methodology over more study areas provides more reliable results in evaluating the performance of an altimeter such as Sentinel-3 SRAL, which is an ongoing objective of our research.

Author Contributions: Conceptualization, P.A., S.R. and B.V.; methodology, P.A., B.V., S.R. and A.A.; software, P.A.; validation, P.A., S.R. and B.V.; formal analysis, P.A., S.R., B.V., A.A. and D.P.; investigation, P.A.; resources, P.A., S.R. and B.V.; data curation, P.A.; writing—original draft preparation, P.A. and S.R.; writing—review and editing, S.R., B.V., P.A., A.A. and D.P.; visualization, P.A.; supervision, B.V.; funding acquisition, D.P. All authors have read and agreed to the published version of the manuscript.

Funding: This research received no external funding.

Data Availability Statement: The Sentinel-3A SAR data can be found through the Europe Space Agency (https://scihub.copernicus.eu/dhus/#/home, accessed on 13 May 2021). The tide gauge data in the Bay of Biscay can be found at http://data.shom.fr/donnes/refmar, accessed on 13 May 2021.

Acknowledgments: We would like to thank the European Space Agency (ESA) and EUMETSAT for providing Sentinel-3A data and the French Réseaux de référence des observations marégraphiques (REFMAR) networks for providing and publishing the unique tide gauge data in the Bay of Biscay. We would also like to acknowledge the DGFI-TUM for providing the ALES dataset.

Conflicts of Interest: The authors declare no conflict of interest.

References

1. Cipollini, P.; Calafat, F.M.; Jevrejeva, S.; Melet, A.; Prandi, P. Monitoring Sea Level in the Coastal Zone with Satellite Altimetry and Tide Gauges. *Surv. Geophys.* **2017**, *38*, 33–57. [CrossRef] [PubMed]
2. Salameh, E.; Frappart, F.; Marieu, V.; Spodar, A.; Parisot, J.-P.; Hanquiez, V.; Turki, I.; Laignel, B. Monitoring Sea Level and Topography of Coastal Lagoons Using Satellite Radar Altimetry: The Example of the Arcachon Bay in the Bay of Biscay. *Remote Sens.* **2018**, *10*, 297. [CrossRef]
3. Benveniste, J.; Cazenave, A.; Vignudelli, S.; Fenoglio-Marc, L.; Shah, R.; Almar, R.; Andersen, O.; Birol, F.; Bonnefond, P.; Bouffard, J.; et al. Requirements for a Coastal Hazards Observing System. *Front. Mar. Sci.* **2019**, *6*, 348. [CrossRef]
4. Benveniste, J.; Birol, F.; Calafat, F.; Cazenave, A.; Dieng, H.; Gouzenes, Y.; Legeais, J.F.; Léger, F.; Niño, F.; Passaro, M.; et al. Coastal sea level anomalies and associated trends from Jason satellite altimetry over 2002–2018. *Sci. Data* **2020**, *7*, 357. [CrossRef]
5. Esselborn, S.; Schöne, T.; Illigner, J.; Weiß, R.; Artz, T.; Huang, X. Validation of Recent Altimeter Missions at Non-Dedicated Tide Gauge Stations in the Southeastern North Sea. *Remote Sens.* **2022**, *14*, 236. [CrossRef]
6. Handoko, E.Y.; Fernandes, M.J.; Lázaro, C. Assessment of Altimetric Range and Geophysical Corrections and Mean Sea Surface Models—Impacts on Sea Level Variability around the Indonesian Seas. *Remote Sens.* **2017**, *9*, 102. [CrossRef]
7. Roohi, S.; Amini, A.; Voosoghi, B.; Battles, D. Lake Monitoring from a Combination of Multi Copernicus Missions: Sentinel-1 A and B and Sentinel-3A. *J. Hydrogeol. Hydrol. Eng.* **2019**, *8*, 3.
8. Vignudelli, S.; Scozzari, A.; Abileah, R.; Gómez-Enri, J.; Benveniste, J.; Cipollini, P. Chapter Four—Water surface elevation in coastal and inland waters using satellite radar altimetry. In *Extreme Hydroclimatic Events and Multivariate Hazards in a Changing Environment*; Maggioni, V., Massari, C., Eds.; Elsevier: Amsterdam, The Netherlands, 2019; pp. 87–127. [CrossRef]

9. Vignudelli, S.; Birol, F.; Benveniste, J.; Fu, L.-L.; Picot, N.; Raynal, M.; Roinard, H. Satellite Altimetry Measurements of Sea Level in the Coastal Zone. *Surv. Geophys.* **2019**, *40*, 1319–1349. [CrossRef]
10. Wang, H.; Huang, Z. Waveform Decontamination for Improving Satellite Radar Altimeter Data Over Nearshore Area: Upgraded Algorithm and Validation. *Front. Earth Sci.* **2021**, *9*, 788. [CrossRef]
11. Brown, G. The average impulse response of a rough surface and its applications. *IEEE Trans. Antennas Propag.* **1977**, *25*, 67–74. [CrossRef]
12. Guo, J.Y.; Guo, Y.G.; Chang, X.C.; Huang, J.W. Optimized threshold algorithm of Envisat waveform retracking over coastal sea. *Chin. J. Geophys.* **2010**, *53*, 807–814. [CrossRef]
13. Wang, X.; Ichikawa, K.; Wei, D. Coastal Waveform Retracking in the Slick-Rich Sulawesi Sea of Indonesia, Based on Variable Footprint Size with Homogeneous Sea Surface Roughness. *Remote Sens.* **2019**, *11*, 1274. [CrossRef]
14. Idris, N.H.; Vignudelli, S.; Deng, X. Assessment of retracked sea levels from Sentinel-3A Synthetic Aperture Radar (SAR) mode altimetry over the marginal seas at Southeast Asia. *Int. J. Remote Sens.* **2021**, *42*, 1535–1555. [CrossRef]
15. Donlon, C.J.; Cullen, R.; Giulicchi, L.; Vuilleumier, P.; Francis, C.R.; Kuschnerus, M.; Simpson, W.; Bouridah, A.; Caleno, M.; Bertoni, R.; et al. The Copernicus Sentinel-6 mission: Enhanced continuity of satellite sea level measurements from space. *Remote Sens. Environ.* **2021**, *258*, 112395. [CrossRef]
16. Raynal, M.; Labroue, S.; Moreau, T.; Boy, F.; Picot, N. From conventional to Delay Doppler altimetry: A demonstration of continuity and improvements with the Cryosat-2 mission. *Adv. Space Res.* **2018**, *62*, 1564–1575. [CrossRef]
17. Wingham, D.J.; Rapley, C.; Griffiths, H.D. New techniques in satellite altimeter tracking systems. In Proceedings of the IGARSS 86 Symposium, Zurich, Switzerland, 8–11 September 1986; Volume 86, pp. 1339–1344.
18. Davis, C.H. Growth of the Greenland ice sheet: A performance assessment of altimeter retracking algorithms. *IEEE Trans. Geosci. Remote Sens.* **1995**, *33*, 1108–1116. [CrossRef]
19. Hwang, C.; Guo, J.; Deng, X.; Hsu, H.-Y.; Liu, Y. Coastal Gravity Anomalies from Retracked Geosat/GM Altimetry: Improvement, Limitation and the Role of Airborne Gravity Data. *J. Geod.* **2006**, *80*, 204–216. [CrossRef]
20. Martin, T.V.; Zwally, H.J.; Brenner, A.C.; Bindschadler, R.A. Analysis and retracking of continental ice sheet radar altimeter waveforms. *J. Geophys. Res. Ocean.* **1983**, *88*, 1608–1616. [CrossRef]
21. Tseng, K.H.; Shum, C.K.; Yi, Y.; Emery, W.J.; Kuo, C.Y.; Lee, H.; Wang, H. The Improved Retrieval of Coastal Sea Surface Heights by Retracking Modified Radar Altimetry Waveforms. *IEEE Trans. Geosci. Remote Sens.* **2014**, *52*, 991–1001. [CrossRef]
22. Huang, Z.; Wang, H.; Luo, Z.; Shum, C.K.; Tseng, K.-H.; Zhong, B. Improving Jason-2 Sea Surface Heights within 10 km Offshore by Retracking Decontaminated Waveforms. *Remote Sens.* **2017**, *9*, 1077. [CrossRef]
23. Roohi, S.; Sneeuw, N.; Benveniste, J.; Dinardo, S.; Issawy, E.A.; Zhang, G. Evaluation of CryoSat-2 water level derived from different retracking scenarios over selected inland water bodies. *Adv. Space Res.* **2019**, *68*, 947–962. [CrossRef]
24. Passaro, M.; Cipollini, P.; Vignudelli, S.; Quartly, G.D.; Snaith, H.M. ALES: A multi-mission adaptive subwaveform retracker for coastal and open ocean altimetry. *Remote Sensing of Environment* **2014**, *145*, 173–189. [CrossRef]
25. Xu, X.-Y.; Birol, F.; Cazenave, A. Evaluation of Coastal Sea Level Offshore Hong Kong from Jason-2 Altimetry. *Remote Sens.* **2018**, *10*, 282.
26. Birol, F.; Léger, F.; Passaro, M.; Cazenave, A.; Niño, F.; Calafat, F.M.; Shaw, A.; Legeais, J.-F.; Gouzenes, Y.; Schwatke, C.; et al. The X-TRACK/ALES multi-mission processing system: New advances in altimetry towards the coast. *Adv. Space Res.* **2021**, *67*, 2398–2415. [CrossRef]
27. Quartly, G.D.; Nencioli, F.; Raynal, M.; Bonnefond, P.; Nilo Garcia, P.; Garcia-Mondéjar, A.; Flores de la Cruz, A.; Crétaux, J.-F.; Taburet, N.; Frery, M.-L.; et al. The Roles of the S3MPC: Monitoring, Validation and Evolution of Sentinel-3 Altimetry Observations. *Remote Sens.* **2020**, *12*, 1763. [CrossRef]
28. Donlon, C.; Berruti, B.; Buongiorno, A.; Ferreira, M.H.; Féménias, P.; Frerick, J.; Goryl, P.; Klein, U.; Laur, H.; Mavrocordatos, C.; et al. The Global Monitoring for Environment and Security (GMES) Sentinel-3 mission. *Remote Sens. Environ.* **2012**, *120*, 37–57. [CrossRef]
29. Sentinel-3 Team. *Sentinel-3 User Handbook*; EUMETSAT: Darmstadt, Germany, 2013.
30. Passaro, M.; Fenoglio-Marc, L.; Cipollini, P. Validation of Significant Wave Height from Improved Satellite Altimetry in the German Bight. *IEEE Trans. Geosci. Remote Sens.* **2015**, *53*, 2146–2156. [CrossRef]
31. Passaro, M.; Smith, W.; Schwatke, C.; Piccioni, G.; Dettmering, D. Validation of a global dataset based on subwaveform retracking: Improving the precision of pulse-limited satellite altimetry. In Proceedings of the 11th Coastal Altimetry Workshop, Frascati, Italy, 13–15 June 2018.
32. Forootan, E.; Rietbroek, R.; Kusche, J.; Sharifi, M.A.; Awange, J.L.; Schmidt, M.; Omondi, P.; Famiglietti, J. Separation of large scale water storage patterns over Iran using GRACE, altimetry and hydrological data. *Remote Sens. Environ.* **2014**, *140*, 580–595. [CrossRef]
33. Kämpf, J.; Sadrinasab, M. The circulation of the Persian Gulf: A numerical study. *Ocean Sci.* **2006**, *2*, 27–41. [CrossRef]
34. Vu, P.L.; Frappart, F.; Darrozes, J.; Marieu, V.; Blarel, F.; Ramillien, G.; Bonnefond, P.; Birol, F. Multi-Satellite Altimeter Validation along the French Atlantic Coast in the Southern Bay of Biscay from ERS-2 to SARAL. *Remote Sens.* **2018**, *10*, 93. [CrossRef]
35. Chelton, D.B.; Ries, J.C.; Haines, B.J.; Fu, L.-L.; Callahan, P.S. Chapter 1 Satellite Altimetry. In *International Geophysics*; Fu, L.-L., Cazenave, A., Eds.; Academic Press: Cambridge, MA, USA, 2001; Volume 69, p. 1-ii.
36. Idris, N.H. Regional validation of the Coastal Altimetry Waveform Retracking Expert System (CAWRES) over the largest archipelago in Southeast Asian seas. *Int. J. Remote Sens.* **2020**, *41*, 5680–5694. [CrossRef]

37. Arabsahebi, R.; Voosoghi, B.; Tourian, M.J. The Inflection-Point Retracking Algorithm: Improved Jason-2 Sea Surface Heights in the Strait of Hormuz. *Mar. Geod.* **2018**, *41*, 331–352. [CrossRef]
38. Fernandes, M.J.; Lázaro, C. Independent Assessment of Sentinel-3A Wet Tropospheric Correction over the Open and Coastal Ocean. *Remote Sens.* **2018**, *10*, 484. [CrossRef]
39. Yuan, J.; Guo, J.; Niu, Y.; Zhu, C.; Li, Z.; Liu, X. Denoising Effect of Jason-1 Altimeter Waveforms with Singular Spectrum Analysis: A Case Study of Modelling Mean Sea Surface Height over South China Sea. *J. Mar. Sci. Eng.* **2020**, *8*, 426. [CrossRef]
40. Roohi, S. Capability of Pulse-Limited Satellite Radar Altimetry to Monitor Inland Water Bodies. Master Thesis, University of Stuttgart, Stuttgart, Germany, 2015.
41. Ganguly, D.; Chander, S.; Desai, S.; Chauhan, P. A Subwaveform-Based Retracker for Multipeak Waveforms: A Case Study over Ukai Dam/Reservoir. *Mar. Geod.* **2015**, *38* (Suppl. 1), 581–596. [CrossRef]
42. Jain, M.; Andersen, O.B.; Dall, J.; Stenseng, L. Sea surface height determination in the Arctic using Cryosat-2 SAR data from primary peak empirical retrackers. *Adv. Space Res.* **2015**, *55*, 40–50. [CrossRef]
43. Jinyum, G.; Cheiway, H.; Xiaotao, C.; Yuting, L. Improved threshold retracker for satellite altimeter waveform retracking over coastal sea. *Prog. Nat. Sci.* **2006**, *16*, 732–738. [CrossRef]
44. Lee, H.; Shum, C.K.; Emery, W.; Calmant, S.; Deng, X.; Kuo, C.-Y.; Roesler, C.; Yi, Y. Validation of Jason-2 Altimeter Data by Waveform Retracking over California Coastal Ocean. *Mar. Geod.* **2010**, *33* (Suppl. 1), 304–316. [CrossRef]

Disclaimer/Publisher's Note: The statements, opinions and data contained in all publications are solely those of the individual author(s) and contributor(s) and not of MDPI and/or the editor(s). MDPI and/or the editor(s) disclaim responsibility for any injury to people or property resulting from any ideas, methods, instructions or products referred to in the content.